Residential Demand Side Management Under High Penetration of Rooftop Photovoltaic Units

Enxin Yao, *Student Member, IEEE*, Pedram Samadi, *Student Member, IEEE*,
Vincent W.S. Wong, *Senior Member, IEEE*, and Robert Schober, *Fellow, IEEE*

***Abstract*—In a residential area where many households have installed rooftop photovoltaic (PV) units, there is a reverse power flow from the households to the substation when the power generation from PV units is larger than the aggregate load of the households. This reverse power flow causes the voltage rise problem. In this paper, we study the use of demand side management (DSM) to mitigate the voltage rise problem. We propose an autonomous energy consumption scheduling algorithm which schedules the operation of deferrable loads to jointly shave the peak load and reduce the reverse power flow. The proposed algorithm shifts the operation of deferrable loads from peak consumption hours to hours with high power generation from the PV units. We use stochastic programming to formulate an energy consumption scheduling problem, which takes into account the uncertainty related to the amount of power generation from PV units. The formulated cost function comprises a monetary cost for energy consumption, the revenue from energy export, and an external cost for the voltage rise. Numerical results show that our proposed algorithm can mitigate the voltage rise problem in areas with high penetration of PV units and reduce the peak-to-average ratio (PAR) of the aggregate load.**

***Index Terms*—Demand side management, optimal scheduling, photovoltaic units, voltage control.**

I. Introduction

Price-based demand side management (DSM) programs encourage users to shift their load from peak consumption hours to off-peak hours in order to reduce the generation cost and the cost of plant investment [1]. Dynamic pricing schemes such as time of use (TOU) pricing are examples of price-based DSM programs in which the utility company sets a high price during peak consumption hours to encourage the users to shift their load from peak hours to off-peak hours.

Residential DSM has attracted significant attention [2]–[6]. An important challenge for residential DSM is that it is difficult for household users to respond to the pricing signals [2]. To tackle this problem, an autonomous energy consumption scheduler (ECS) can be implemented to help users make price-based control decisions. The autonomous ECS retrieves the pricing signal from the utility company via a communication infrastructure and schedules the operation of deferrable loads such as electric water heaters and clothes dryers. The authors of [3]–[6] propose algorithms to schedule the residential load and minimize the electricity bill.

In recent years, the use of rooftop photovoltaic (PV) units and energy storage systems (ESSs) in households has proliferated. The households may not only consume energy but also export energy to the power grid. Many utility companies use net metering programs to encourage households to install rooftop PV units [7], [8]. Net metering programs typically have a feed-in tariff and allow households to sell their extra energy to the power grid. In [9], a coordinated algorithm is proposed to minimize the users' payments. The proposed algorithm in [9] controls both the household load and distributed energy resources (DERs) (e.g., PV units). A game-theoretic approach is proposed in [10] which jointly controls the load, DERs, and ESSs. In [11], an energy consumption scheduling algorithm is proposed for a PV-based microgrid, where the time of use probabilities of different loads are considered. The works in [9]–[11] focus on the case where a few households are equipped with DER units and are encouraged to export their generation to the grid. However, if a large number of users are equipped with PV units, the results in [9]–[11] may not be directly applicable because the reverse power flow in those areas may cause the *voltage rise* problem. Therefore, in areas with high penetration of PV units, new DSM programs are necessary.

The voltage rise problem is an important challenge for the integration of a large number of rooftop PV units into the power grid [12], [13]. Traditional voltage control strategies assume the unidirectional power flow from the substation to the households [14]. A substantial reverse power flow from households to the substation can cause the voltage magnitude of some of the households to exceed the upper limit of the allowed voltage variation. This is referred to as the voltage rise problem. For example, in North America, the ANSI C84.1 standard [15] requires the voltage magnitude in the distribution network to be no more than 1.05 per unit (pu) of the normal state. For the rest of the paper, we assume that the upper limit for the allowed voltage variation is 1.05 pu.

In countries such as Germany with high penetration of rooftop PV units, the voltage rise problem has already emerged and different mechanisms have been proposed to tackle the problem [16], [17]. The distribution network operators (DNOs) have upgraded the transformers (e.g., with on-load tap changer transformers) and have enhanced the feeder to host more PV units in some areas [16]. Moreover, the reverse power flow from PV units can be controlled by adjusting the active and reactive power of PV inverters [17]. In particular, the

Manuscript was received on Nov. 1, 2014, revised on Apr. 10, 2015 and July 7, 2015, and accepted on Aug. 17, 2015. This work is supported by the Natural Sciences and Engineering Research Council of Canada (NSERC) under Strategic Project Grant (STPGP 447607-13). E. Yao, P. Samadi, V.W.S. Wong, and R. Schober are with the Department of Electrical and Computer Engineering, The University of British Columbia, Vancouver, Canada, email: {enxinyao, psamadi, vincentw, rschober}@ece.ubc.ca.

German Renewable Energy Sources Act revision in 2012 [18] enforces energy generation curtailment for rooftop PV units. The DNO measures the voltage magnitude and sends control signals to the PV units for curtailment. The PV units are required to either install remote controllers that curtail the generation based on the control signal received from the DNO or permanently limit the active power feed-in to 70% of the installed capacity [16].

Besides generation curtailment, load control techniques and ESSs (e.g., battery systems) can be used to reduce the reverse power flow during high solar radiation hours and mitigate the voltage rise problem [19]–[23]. The work in [19] proposes the activation of additional heating, ventilation, and air conditioning (HVAC) load whenever a voltage rise is detected. The works in [20]–[22] focus on using ESSs to mitigate the voltage rise problem. ESSs can absorb the reverse power flow when the voltage rise is detected. However, the control of residential load and ESSs requires the approval of household owners. Economic incentives such as TOU pricing should be considered in the DSM programs to encourage household participation. On the other hand, the voltage rise problem should also be taken into account in DSM programs if many households are equipped with PV units. Moreover, it is hard to respond to variations of voltage and pricing signals manually. Hence, it is important to have a scheduling algorithm for an autonomous ECS to manage load and ESSs without human intervention.

The contributions of this work are as follows:

- We propose a residential energy consumption scheduling algorithm for areas with high penetration of rooftop PV units. The proposed algorithm aims to reduce the energy expenses of the users and mitigate the voltage rise problem. It shifts deferrable load from peak consumption hours to hours with high solar power generation.
- We introduce a cost function to model the undesired voltage rise. The objective function comprises a monetary cost for household energy consumption, the energy generation revenue from PV units, and an external cost for the voltage rise. The external cost is modeled with the sensitivity of the voltage magnitudes with respect to the household energy export, which can be obtained from power flow analysis. We formulate a stochastic energy consumption scheduling problem to minimize the cost function. We transform the problem into a linear program (LP) when the feed-in tariff does not exceed the energy consumption price and the cost function is convex piecewise linear. Otherwise, when the cost function is non-convex, a mixed-integer program (MIP) is formulated.
- We compare our proposed algorithm with the algorithm in [19] on a 33 bus radial distribution test system. Simulation results show that our proposed algorithm reduces the energy expenses of the users. The results also show that our algorithm can mitigate the voltage rise problem for areas with high penetration of PV units and reduce the peak-to-average ratio (PAR) of the aggregate load.

The rest of the paper is organized as follows. The system model is introduced in Section II. In Section III, we present the problem formulation and the proposed algorithm. Numerical results are presented in Section IV, and conclusions are drawn in Section V.

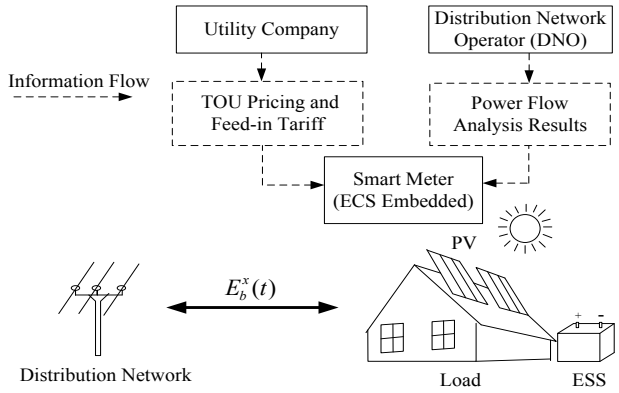

Fig. 1. A schematic diagram of the proposed energy consumption scheduling scheme. The DNO performs the power flow analysis and provides the ECS with information regarding the voltage rise (e.g., the sensitivity of the voltage with respect to the household energy export) at the beginning of the day.

II. System Model

A block diagram of the proposed energy consumption scheduling scheme for a household equipped with a PV unit and an ESS is shown in Fig. 1. The power flows from the distribution network to the load when the power generated by the PV unit is insufficient to meet the demand. The direction of the power flow is reversed when the power generated by the PV unit is higher than the load. Each household is equipped with an ECS [2], which is embedded in the household smart meter. The ECS retrieves the pricing information from the utility company. A DNO performs the power flow analysis [14] for the local distribution network and determines the hours when the households may have abnormally high voltage magnitude if load shifting is not performed. We assume the DNO performs the power flow analysis based on historical records of demand and generation. The DNO sends the power flow analysis results to the ECS at the beginning of each day. The ECS determines the operational schedule of the *deferrable load* to minimize the electricity bill and reduce the reverse power flow for hours when voltage rise may happen. Examples of such deferrable load include clothes dryers and electric water heaters. Some other loads such as TV and computers are *must-run load* [5] because their energy consumption cannot be shifted. We also consider the ESSs in our model, e.g., battery systems owned by the household. We denote the sets of deferrable load, must-run load, and ESSs by $\mathcal{S}^d$, $\mathcal{S}^m$, and $\mathcal{S}^s$, respectively. We note that the demand and PV energy generation are stochastic in practice and can be different from the values obtained from the historical records. This may introduce inaccuracy when the DNO performs the power flow analysis. In Section IV, we analyze the effect of forecast errors via simulations.

We denote the set of operating time slots under consideration by $\mathcal{T} \triangleq \{1, \ldots, T\}$. The selection of an appropriate length of the time slot depends on the formulated problem. On the

one hand, a relatively short time slot is helpful to model the dynamics of the load and the energy generation of PV units. Short time slots make the assumption that the active power, reactive power, and phase on the buses are static within one time slot more realistic. On the other hand, longer time slots reduce the computational complexity of the algorithm. In this paper, we choose the length of a time slot to be 15 minutes in order to achieve a balance between the performance and the complexity of the algorithm. Furthermore, we use $E_i^d(t)$, $E_j^m(t)$, and $E_l^s(t)$ to denote the energy consumption of the deferrable load $i \in \mathcal{S}^d$, the energy consumption of the must-run load $j \in \mathcal{S}^m$, and the charged or discharged energy of the ESS $l \in \mathcal{S}^s$ at time slot $t \in \mathcal{T}$, respectively. The energy generated from PV units at time slot t is denoted by $E^g(t)$. For a household connected to bus b, the exported energy at time slot t is denoted by $E_b^x(t)$ and is given by

$$E_b^x(t) = E^g(t) - \sum_{i \in \mathcal{S}^d} E_i^d(t) - \sum_{j \in \mathcal{S}^m} E_j^m(t) - \sum_{l \in \mathcal{S}^s} E_l^s(t). \quad (1)$$

The ECS adjusts $E_b^x(t)$ by controlling the operation of deferrable loads and ESSs. Let $\mathbf{e}_t$ represent the vector of the energy consumption of the deferrable loads and the charged or discharged energy of the ESSs at time slot t. $\mathbf{e}_t$ can be written as

$$\mathbf{e}_t = (E_1^d(t), \ldots, E_{|\mathcal{S}^d|}^d(t), E_1^s(t), \ldots, E_{|\mathcal{S}^s|}^s(t)), \quad (2)$$

where $|\mathcal{S}^d|$ and $|\mathcal{S}^s|$ are the cardinalities of sets $\mathcal{S}^d$ and $\mathcal{S}^s$, respectively. We model the PV units as non-controllable resources because household rooftop PV units are typically non-dispatchable [13]. Moreover, rooftop PV units are required to operate with unity power factor according to the current IEEE 1547 standard [24]. We restrict our model to consider the active power generation (i.e., $E^g(t)$) of PV units.

A. Voltage Rise Problem

The voltage rise problem occurs when many households in the distribution network have large positive $E_b^x(t)$. A 33 bus radial distribution network [25] is shown in Fig. 2. The households are connected to the buses. We denote the set of buses as $\mathcal{B}$ (e.g., $\mathcal{B} = \{1, \ldots, 33\}$ in Fig. 2). We denote the voltage magnitude on bus $n \in \mathcal{B}$ as $|V_n(t)|$. Note that we use b to specify the bus to which the considered household is connected, whereas bus n is an arbitrary bus. The value of $|V_n(t)|$ is determined using the power flow analysis. We assume the active power, reactive power, voltage magnitude, and phase are static within one time slot. We first consider the case when load shifting is not performed. The DNO executes the power flow analysis using historical records of demand and generation. In this case, $|V_n(t)|$ may exceed an upper limit (e.g., 1.05 pu in North America) on some of the buses. Hence, we obtain a set of buses with abnormally high voltage magnitude in time slot t, which is denoted by $\mathcal{B}^v(t)$. We aim to decrease the voltage magnitude $|V_n(t)|$ of buses $n \in \mathcal{B}^v(t)$ by decreasing $E_b^x(t)$ via load shifting, when $\mathcal{B}^v(t)$ is not $\emptyset$.

The sensitivity of the voltage magnitude $|V_n(t)|$ of an arbitrary bus n with respect to household energy export $E_b^x(t)$ is characterized by the partial derivative $\frac{\partial |V_n(t)|}{\partial E_b^x(t)}$. We note that $|V_n(t)|$ depends on the power flow of all the buses. Moreover, a non-convex problem has to be solved to obtain $|V_n(t)|$. However, in order to reduce the computational complexity, a linear model of the external cost is adopted, and the partial derivatives $\frac{\partial |V_n(t)|}{\partial E_b^x(t)}$ are used to analyze the sensitivity of $|V_n(t)|$ with respect to $E_b^x(t)$. $\frac{\partial |V_n(t)|}{\partial E_b^x(t)}$ is obtained from power flow analysis using the Newton-Raphson method [14]. That is, the Newton-Raphson method is used to obtain the Jacobian matrix which contains the information about the partial derivatives of the active and reactive powers with respect to the voltage magnitude and phase. Next, the partial derivative $\frac{\partial |V_n(t)|}{\partial E_b^x(t)}$ is obtained from the inverse of the Jacobian matrix [26], [27]. The exact values can be calculated using off-the-shelf software such as PowerWorld [28] or Matlab. We assume the DNO performs the power flow analysis based on the historical records of demand and generation. The DNO sends the results, i.e., $\frac{\partial |V_n(t)|}{\partial E_b^x(t)}$ and $|V_n(t)|$, to the ECS as the input for the energy consumption scheduling algorithm.

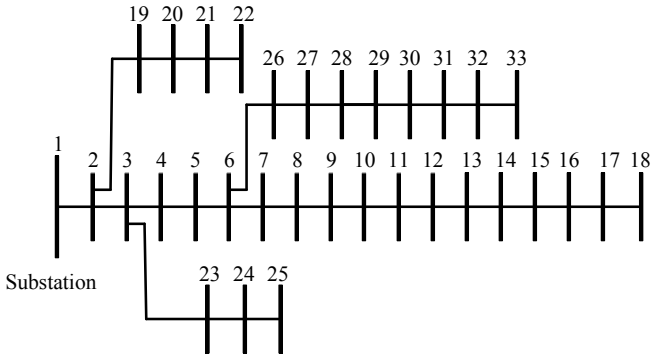

Fig. 2. One line diagram of a 33 bus radial distribution test system [25]. The households are connected to the buses. The voltage rise problem occurs when many households have substantial positive energy export. The DSM program encourages households to shift loads to hours with high solar radiation to mitigate the voltage rise problem.

B. Cost Function

The energy export of a household on an arbitrary bus b may contribute to the voltage rise problem of other households in the distribution network (including the households on other buses). We model the contribution of the household energy export to the abnormally high voltage magnitude of other households as an external cost. In economics, an externality arises when a person engages in an activity that influences the well-being of a bystander [29]. We assume the household aims to minimize its own electricity bill and its external cost.

To tackle the voltage rise problem, the DNO can encourage households to reduce the exported energy to be less than a certain threshold h in each time slot. The DNO determines the value of h by running the power flow analysis in an iterative manner. The power flow analysis is used to determine the bus voltage magnitude. In this analysis, the DNO first sets the energy export from each household to be zero and runs the power flow analysis. In this case, the voltage magnitude on

each bus is lower than 1.05 pu. Then, the DNO gradually increases the energy export of all households simultaneously and repeats the power flow analysis to obtain the voltage magnitude for different energy exports. As the energy export increases, the voltage magnitude obtained in the power flow analysis increases as well. When the voltage magnitude of any bus reaches 1.05 pu, the DNO stops increasing the energy export and the obtained value of the energy export can be used as the value of threshold h. The value of h depends on the voltage magnitude on the secondary winding of the substation transformer, the line impedance, the line length between adjacent buses, and the number of households connected to each bus. These values are used as inputs in the power flow analysis to calculate the voltage magnitude. The value of h should be determined by the DNO for each distribution network according to its specific parameters.

Hence, all households should have the same threshold h to ensure fairness. Parameter h is used as a threshold to obtain the external cost rather than a limit for the energy export. Although households with different PV units can export different amount of energy [30], the prices and threshold h should be the same for the energy export of all households. This is because all households have equal rights to use the public distribution network.

Consider an arbitrary household connected to bus $b \in \mathcal{B}$, we model the external cost of the household energy export as

$$c^x(\mathbf{e}_t) = \eta\Big(\sum_{n\in\mathcal{B}^v(t)} \frac{\partial|V_n(t)|}{\partial E_b^x(t)}\Big)\left[E_b^x(t) - h\right]^+, \qquad (3)$$

where $[x]^+ = \max\{x, 0\}$. $\sum_{n\in\mathcal{B}^v(t)} \frac{\partial|V_n(t)|}{\partial E_b^x(t)}$ is the contribution of one unit household energy export to the abnormally high voltage magnitude of the buses $n \in \mathcal{B}^v(t)$. Note that in practice, voltage rise happens on some of the buses, i.e., the buses in set $\mathcal{B}^v(t)$. The parameter η is a non-negative coefficient. Note that (3) is obtained using a sensitivity-based linear model of the voltage rise. The first order derivative $\frac{\partial|V_n(t)|}{\partial E_b^x(t)}$ models the sensitivity of the voltage magnitude with respect to the power flows. The sensitivity-based linear model has been widely used to study the voltage rise problem [26], [27], [31], [32]. The accuracy of the model may degrade when power flows and voltage deviate from their expected values significantly.

Assume the ECS aims to reduce the monetary cost (i.e., the electricity bill) and the external cost[1]. The household purchases energy at price $p^e(t)$ when $E_b^x(t) < 0$ and sells energy with a feed-in tariff $p^s(t)$ when $E_b^x(t) \geq 0$. The total cost at time slot t is given by

$$c(\mathbf{e}_t)=\begin{cases}\eta\sum\limits_{n\in\mathcal{B}^v(t)}\frac{\partial|V_n(t)|}{\partial E_b^x(t)}(E_b^x(t)-h)-p^s(t)E_b^x(t), & \text{if } E_b^x(t)\geq h,\\ -p^s(t)E_b^x(t), & \text{if } 0\leq E_b^x(t)<h,\\ p^e(t)|E_b^x(t)|, & \text{if } E_b^x(t)<0,\end{cases} \qquad (4)$$

where $|E_b^x(t)|$ represents the absolute value of $E_b^x(t)$. Parameter η can be tuned to adjust the weight between the external cost and the monetary cost. By increasing η, the ECS tends to shift more load to the high solar radiation hours to reduce the external cost of the voltage rise problem. By decreasing η, the ECS puts more weight on minimizing the electricity bill. When $\eta = 0$, the ECS only aims at minimizing the bill and neglects the potential voltage rise problem. Fig. 3 shows that cost function $c(\mathbf{e}_t)$ is a convex piecewise linear function [38] when $p^s(t) \leq p^e(t)$. However, it becomes a non-convex piecewise linear function when $p^s(t) > p^e(t)$. Both cases will be considered in Section III.

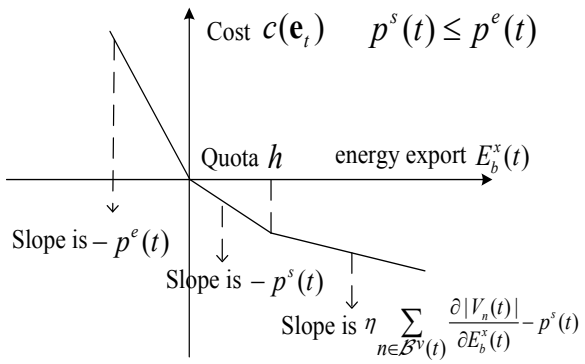

Fig. 3. Piecewise linear cost function for a household with PV unit. We consider the case $p^s(t) \leq p^e(t)$ in this figure, i.e., the feed-in tariff does not exceed the energy consumption price. Note that some utility companies promote the rooftop PV installation aggressively and have $p^s(t) > p^e(t)$ (e.g., [8]).

The households schedule their load in a distributed manner. Distributed load control algorithms are preferred as they reduce the computational complexity and offer more privacy compared to centralized algorithms. We investigate the energy consumption scheduling problem for the ECS by an arbitrary household.

III. Energy Consumption Scheduling with Uncertain PV Power Generation

In this section, we consider the energy consumption scheduling problem for minimizing the expected payment and external cost of the user. We formulate the problem as a *stochastic programming problem* [39]. The uncertainty in the power generation from PV units is taken into account in our formulation. Note that the PV power generation $E^g(t)$ is intermittent and random in nature [40]–[42]. The ECS needs to determine $\mathbf{e}_t$ at the current time slot t, before the future PV power generation $E^g(t+1), \ldots, E^g(T)$ can be observed. In the next time slot, $t+1$, the power consumption vector $\mathbf{e}_{t+1}$ will be updated as the new information about the PV power generation is received.

[1]One promising method to enforce the households to consider the external cost is the monetization of the external cost [33], which has been used in several areas [34]–[37], such as the carbon emission tax in the energy generation. This concept can be used for those areas with high rooftop PV penetration. The external cost can be incurred to the user by means of a carefully selected price function. For example, the utility company may collect an additional charge from households with an energy export exceeding the threshold h. Some utility companies (e.g., Georgia Power) have already been collecting a monthly charge from households which connect their rooftop PV units to the distribution network. Note that with the advanced metering infrastructure (AMI), the utility company can monitor the household energy export in short time intervals and determine the external cost according to the energy export.

For the rest of this paper, we denote the current time slot by t, whereas τ represents an arbitrary time slot. We define $\mathcal{T}_t \triangleq \{t, \ldots, T\}$ as the set of time slots from the current time slot t onwards.

A. Nested Stochastic Formulation

For current time slot t, we define $E_i^r(t)$ as the amount of energy required to finish the operation of appliance $i \in \mathcal{S}^d$. The energy requirement $E_i^r(t)$ is updated as

$$E_i^r(t+1) = \max\Big\{E_i^r(t) - E_i^d(t), 0\Big\}, \quad i \in \mathcal{S}^d. \tag{5}$$

We denote the maximum energy consumption of the ith deferrable load within one time slot by $E_{i,d}^{\max}$. Moreover, $E_{l,s}^{\max} \geq 0$ represents the maximum energy that can be stored in ESS l during one time slot. $E_{l,s}^{\min} \leq 0$ is the maximum energy that can be derived from ESS l during one time slot. We denote the state of charge (SOC) of ESS l at time slot t by $s_l(t)$. The battery capacity of ESS l is denoted by b_l. For ESS l, its SOC is updated as

$$s_l(t) = s_l(t-1) + \frac{E_l^s(t)}{b_l}, \quad l \in \mathcal{S}^s. \tag{6}$$

At current time slot t, the ECS optimizes $\mathbf{e}_t$ for minimization of the cost from the current time slot t onwards. The *nested* form of our stochastic problem is

$$\underset{\mathbf{e}_t \in \chi_t}{\text{minimize}}\ c(\mathbf{e}_t) + \mathbb{E}\left[\inf_{\mathbf{e}_{t+1} \in \chi_{t+1}} c(\mathbf{e}_{t+1}) + \cdots + \mathbb{E}\Big[\inf_{\mathbf{e}_T \in \chi_T} c(\mathbf{e}_T)\Big]\right] \tag{7a}$$

$$\text{subject to } \sum_{\tau=t}^{T_i^d} E_i^d(\tau) = E_i^r(t), \quad i \in \mathcal{S}^d, \tag{7b}$$

where T_i^d is the deadline by which the operation of deferrable load $i \in \mathcal{S}^d$ has to be finished. $\mathbb{E}$ represents the expectation with respect to the uncertain PV power generation. Note that the must-run load may also have uncertainty, depending on how accurately we can forecast the must-run load profile. We also assume that the household users determine the operational constraints of each appliance. The feasible set, $\chi_\tau, \tau \in \mathcal{T}_t$, in (7a) can be written as

$$\begin{aligned}\chi_\tau = \{\ \mathbf{e}_\tau \mid\ & 0 \leq E_i^d(\tau) \leq E_{i,d}^{\max},\ \forall\, i \in \mathcal{S}^d, \\ & E_{l,s}^{\min} \leq E_l^s(\tau) \leq E_{l,s}^{\max},\ \forall\, l \in \mathcal{S}^s, \\ & S^{\min} \leq s_l(\tau) \leq 1,\ \forall\, l \in \mathcal{S}^s\ \}. \end{aligned} \tag{8}$$

The first two constraints in (8) ensure that the energy consumption of load i and charged or discharged energy of ESS l at hour τ do not exceed their respective maximal values. The third constraint prevents the ESS from discharging to an overly low SOC, where $S^{\min}$ is the minimum SOC of the ESS, e.g., $S^{\min} = 0.3$. Note that discharging an ESS to an overly low SOC may degrade the life cycle of the ESS.

Problem (7) is difficult to solve directly. Hence, we adopt the sample average approximation (SAA) technique [39] to solve problem (7).

B. Sample Average Approximation

The SAA technique generates scenarios for unknown future PV power generation and evaluates the objective function by averaging over different scenarios. Suppose we have K scenarios $\{\boldsymbol{\omega}_1, \ldots, \boldsymbol{\omega}_K\}$ based on the historical records of the PV power generation. Each scenario is a possible realization of $(E^g(t+1), \ldots, E^g(T))$. For the kth scenario $\boldsymbol{\omega}_k$, the hourly PV power generation is denoted as $(E^g(t+1, \boldsymbol{\omega}_k), \ldots, E^g(T, \boldsymbol{\omega}_k))$, where $E^g(\tau, \boldsymbol{\omega}_k), \tau \in \mathcal{T}_{t+1}$, is the value of $E^g(\tau)$ under scenario $\boldsymbol{\omega}_k$. We define $\mathcal{K} \triangleq \{1, \ldots, K\}$ as the set of scenarios. For an arbitrary scenario $k \in \mathcal{K}$, let $E_i^d(\tau, \boldsymbol{\omega}_k)$, $E_j^m(\tau, \boldsymbol{\omega}_k)$, $E_l^s(\tau, \boldsymbol{\omega}_k)$, $E_b^x(\tau, \boldsymbol{\omega}_k)$, $s_l(\tau, \boldsymbol{\omega}_k)$, and $\mathbf{e}(\tau, \boldsymbol{\omega}_k)$ denote the energy consumption of the ith deferrable load, the energy consumption of the jth must-run load, the charged or discharged energy of the lth ESS, the household energy export, the SOC of the lth ESS, and the energy consumption vector at time slot τ under scenario $\boldsymbol{\omega}_k$, respectively.

We estimate the expected cost by averaging the cost over different scenarios $\boldsymbol{\omega}_k, \forall\, k \in \mathcal{K}$. By using the SAA technique, problem (7) becomes

$$\underset{\substack{\mathbf{e}(\tau, \boldsymbol{\omega}_k),\\ \tau \in \mathcal{T}_t, k \in \mathcal{K}}}{\text{minimize}} \sum_{k \in \mathcal{K}} \mathbb{P}(\boldsymbol{\omega}_k) \sum_{\tau \in \mathcal{T}_t} c(\mathbf{e}(\tau, \boldsymbol{\omega}_k)) \tag{9a}$$

$$\text{subject to } \sum_{\tau=t}^{T_i^d} E_i^d(\tau, \boldsymbol{\omega}_k) = E_i^r(t), \quad i \in \mathcal{S}^d, \quad k \in \mathcal{K}, \tag{9b}$$

$$0 \leq E_i^d(\tau, \boldsymbol{\omega}_k) \leq E_{i,d}^{\max}, \quad i \in \mathcal{S}^d, \quad \tau \in \mathcal{T}_t, \quad k \in \mathcal{K}, \tag{9c}$$

$$E_{l,s}^{\min} \leq E_l^s(\tau, \boldsymbol{\omega}_k) \leq E_{l,s}^{\max}, \quad l \in \mathcal{S}^s, \quad \tau \in \mathcal{T}_t, \quad k \in \mathcal{K}, \tag{9d}$$

$$S^{\min} \leq s_l(\tau, \boldsymbol{\omega}_k) \leq 1, \quad l \in \mathcal{S}^s, \quad \tau \in \mathcal{T}_t, \quad k \in \mathcal{K}, \tag{9e}$$

$$\mathbf{e}(t, \boldsymbol{\omega}_k) = \mathbf{e}(t, \boldsymbol{\omega}_l), \quad k, l \in \mathcal{K}. \tag{9f}$$

The term $\mathbf{e}(\tau, \boldsymbol{\omega}_k)$ is the energy consumption vector of controllable loads and ESSs at time slot τ under scenario $\boldsymbol{\omega}_k$. $c(\mathbf{e}(\tau, \boldsymbol{\omega}_k))$ denotes the cost function in time slot τ under scenario $\boldsymbol{\omega}_k$. $\sum_{\tau \in \mathcal{T}_t} c(\mathbf{e}(\tau, \boldsymbol{\omega}_k))$ in (9a) indicates the total cost under scenario $\boldsymbol{\omega}_k$ from time slot t to time slot T. The objective function (9a) is the cost from time slot t onwards, averaged across the K scenarios. Constraints (9b) – (9e) are the extensions of the constraints in (7b) and (8) under scenario $\boldsymbol{\omega}_k$. Constraint (9f) is the non-anticipativity constraint of stochastic programming [39]. Note that t in constraint (9f) is the current time slot while τ in problem (9) denotes an arbitrary time slot. Constraint (9f) reflects the fact that the ECS is required to make a deterministic decision in the current time slot before the unknown parameters are revealed. Constraint (9f) enforces the variables of the current time slot t to be equal under different scenarios, such that the obtained solution in the current time slot t is deterministic, i.e., does not depend on a specific scenario. Problem (9) has an objective function which can be either convex or non-convex piecewise linear. For both the convex and non-convex cases, problem (9) will be studied in the following subsections.

C. Convex Piecewise Linear Objective Function

First, we consider the case for which $p^s(\tau) \leq p^e(\tau), \tau \in \mathcal{T}_t$. Fig. 3 illustrates the cost function for this case. The cost function $c(\mathbf{e}(\tau, \boldsymbol{\omega}_k))$ is a convex piecewise linear function since $c(\mathbf{e}(\tau, \boldsymbol{\omega}_k))$ in (4) can be written as

$$c(\mathbf{e}(\tau, \boldsymbol{\omega}_k)) = \max\Big\{ -p^s(\tau)h + \Big((\eta \sum_{n \in \mathcal{B}^v(\tau)} \frac{\partial |V_n(\tau)|}{\partial E_b^x(\tau)} - p^s(\tau)) (E_b^x(\tau, \boldsymbol{\omega}_k) - h)\Big), -p^s(\tau) E_b^x(\tau, \boldsymbol{\omega}_k), p^e(\tau)(-E_b^x(\tau, \boldsymbol{\omega}_k))\Big\}. \tag{10}$$

By introducing auxiliary variables $u(\tau, \boldsymbol{\omega}_k), \tau \in \mathcal{T}_t, k \in \mathcal{K}$, problem (9) can be rewritten as

$$\underset{\substack{\mathbf{e}(\tau,\boldsymbol{\omega}_k), u(\tau,\boldsymbol{\omega}_k), \\ \tau \in \mathcal{T}_t, k \in \mathcal{K}}}{\text{minimize}} \quad \sum_{k \in \mathcal{K}} \mathbb{P}(\boldsymbol{\omega}_k) \sum_{\tau \in \mathcal{T}_t} u(\tau, \boldsymbol{\omega}_k) \tag{11a}$$

$$\text{subject to} \quad u(\tau, \boldsymbol{\omega}_k) \geq -p^s(\tau)h + \Big((\eta \sum_{n \in \mathcal{B}^v(\tau)} \frac{\partial |V_n(\tau)|}{\partial E_b^x(\tau)} - p^s(\tau))(E_b^x(\tau, \boldsymbol{\omega}_k) - h)\Big), \ \tau \in \mathcal{T}_t, \quad k \in \mathcal{K}, \tag{11b}$$

$$u(\tau, \boldsymbol{\omega}_k) \geq -p^s(\tau) E_b^x(\tau, \boldsymbol{\omega}_k), \ \tau \in \mathcal{T}_t, \quad k \in \mathcal{K}, \tag{11c}$$

$$u(\tau, \boldsymbol{\omega}_k) \geq p^e(\tau)(-E_b^x(\tau, \boldsymbol{\omega}_k)), \quad \tau \in \mathcal{T}_t, \quad k \in \mathcal{K}, \tag{11d}$$

Constraints (9b) – (9e).

The linear constraints (11b) – (11d) are introduced to replace the piecewise linear objective function $c(\mathbf{e}(\tau, \boldsymbol{\omega}_k))$ in (10). Problem (11) is a linear program (LP) and can be solved efficiently.

D. Non-convex Piecewise Linear Objective Function

For the case in which $p^s(\tau) > p^e(\tau), \tau \in \mathcal{T}_t$, the cost function is a non-convex piecewise linear function, cf. Fig. 4. The high feed-in tariff is typically used to encourage households to install rooftop PV units. For example, in the province of Ontario in Canada, the feed-in tariff for rooftop PV units is $32.9 - 39.6$ cents per kWh [8] while the residential energy consumption price is $7.2 - 12.9$ cents per kWh. Moreover, in the state of Georgia in the United States, the utility company has a residential energy retailing price of $4.8 - 9.6$ cents per kWh while purchases energy from rooftop PV units at 17 cents per kWh [43]. The high feed-in tariff in the province of Ontario in Canada and Georgia state in the United States are for the roof-top PV units only.

A non-convex piecewise linear objective function cannot be directly transformed into an LP. To tackle problem (9) with a non-convex piecewise linear objective function, we introduce new variables $q_0(\tau, \boldsymbol{\omega}_k)$, $q_1(\tau, \boldsymbol{\omega}_k)$, and $q_2(\tau, \boldsymbol{\omega}_k)$ to represent the components of energy export $E_b^x(\tau, \boldsymbol{\omega}_k)$ in the three different pricing ranges, cf. Fig. 4. Then, we have

$$q_0(\tau, \boldsymbol{\omega}_k) = \min\{ E_b^x(\tau, \boldsymbol{\omega}_k) - H, |H| \}, \tag{12}$$

$$q_1(\tau, \boldsymbol{\omega}_k) = \min\{\max\{ E_b^x(\tau, \boldsymbol{\omega}_k), 0 \}, h\}, \tag{13}$$

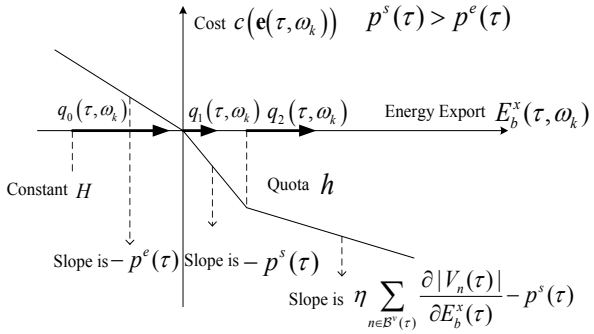

Fig. 4. Non-convex piecewise linear cost function. This case occurs when the feed-in tariff of the utility company is higher than the energy consumption price (i.e., $p^s(\tau) > p^e(\tau)$) [8].

$$q_2(\tau, \boldsymbol{\omega}_k) = \max\{ E_b^x(\tau, \boldsymbol{\omega}_k) - h, 0 \}, \tag{14}$$

$$E_b^x(\tau, \boldsymbol{\omega}_k) = (H + q_0(\tau, \boldsymbol{\omega}_k)) + q_1(\tau, \boldsymbol{\omega}_k) + q_2(\tau, \boldsymbol{\omega}_k), \tag{15}$$

$$c(\mathbf{e}(\tau, \boldsymbol{\omega}_k)) = p^e(\tau)(|H| - q_0(\tau, \boldsymbol{\omega}_k)) - p^s(\tau) q_1(\tau, \boldsymbol{\omega}_k) - (p^s(\tau) - \eta \sum_{n \in \mathcal{B}^v(\tau)} \frac{\partial |V_n(\tau)|}{\partial E_b^x(\tau)}) q_2(\tau, \boldsymbol{\omega}_k), \tag{16}$$

where H is a negative constant, cf. Fig. 4. The value of H is selected to be less than the minimum of $E_b^x(\tau, \boldsymbol{\omega}_k)$. Now, problem (9) can be rewritten as

$$\underset{\substack{\mathbf{e}(\tau,\boldsymbol{\omega}_k), q_0(\tau,\boldsymbol{\omega}_k), \\ q_1(\tau,\boldsymbol{\omega}_k), q_2(\tau,\boldsymbol{\omega}_k), \\ \tau \in \mathcal{T}_t, k \in \mathcal{K}}}{\text{minimize}} \quad \sum_{k \in \mathcal{K}} \mathbb{P}(\boldsymbol{\omega}_k) \sum_{\tau \in \mathcal{T}_t} \Big(p^e(\tau)(|H| - q_0(\tau, \boldsymbol{\omega}_k)) - p^s(\tau) q_1(\tau, \boldsymbol{\omega}_k) - \big(p^s(\tau) - \eta \sum_{n \in \mathcal{B}^v(\tau)} \frac{\partial |V_n(\tau)|}{\partial E_b^x(\tau)}\big) q_2(\tau, \boldsymbol{\omega}_k)\Big) \tag{17a}$$

$$\text{subject to} \quad 0 \leq q_0(\tau, \boldsymbol{\omega}_k) \leq |H|, \ \tau \in \mathcal{T}_t, \ k \in \mathcal{K}, \tag{17b}$$

$$0 \leq q_1(\tau, \boldsymbol{\omega}_k) \leq h, \quad \tau \in \mathcal{T}_t, \quad k \in \mathcal{K}, \tag{17c}$$

$$0 \leq q_2(\tau, \boldsymbol{\omega}_k), \quad \tau \in \mathcal{T}_t, \quad k \in \mathcal{K}, \tag{17d}$$

$$q_1(\tau, \boldsymbol{\omega}_k)(q_0(\tau, \boldsymbol{\omega}_k) - |H|) = 0, \quad \tau \in \mathcal{T}_t, \quad k \in \mathcal{K}, \tag{17e}$$

$$q_2(\tau, \boldsymbol{\omega}_k)(q_1(\tau, \boldsymbol{\omega}_k) - h) = 0, \quad \tau \in \mathcal{T}_t, \quad k \in \mathcal{K}, \tag{17f}$$

$$\sum_{i \in \mathcal{S}^d} E_i^d(\tau, \boldsymbol{\omega}_k) + \sum_{j \in \mathcal{S}^m} E_j^m(\tau, \boldsymbol{\omega}_k) + \sum_{l \in \mathcal{S}^s} E_l^s(\tau, \boldsymbol{\omega}_k) \geq 0, \ \tau \in \mathcal{T}_t, \quad k \in \mathcal{K}, \tag{17g}$$

Constraints (9b) – (9e), and (15).

Constraints (17b) – (17d) ensure that $q_0(\tau, \boldsymbol{\omega}_k)$, $q_1(\tau, \boldsymbol{\omega}_k)$, and $q_2(\tau, \boldsymbol{\omega}_k)$ are selected within their ranges. Because of constraint (17e), $q_1(\tau, \boldsymbol{\omega}_k)$ can have a non-zero value only if $q_0(\tau, \boldsymbol{\omega}_k)$ has reached its maximum. Similarly, because of constraint (17f), $q_2(\tau, \boldsymbol{\omega}_k)$ can be non-zero only if $q_1(\tau, \boldsymbol{\omega}_k)$ has reached its maximum. Constraint (17g) ensures that, under high feed-in tariff, the households export energy from their PV units rather than their ESSs. Note that both Ontario Hydro and Georgia Power [8], [43] restrict that only the energy export from certain types of renewable resources are eligible for high

feed-in tariff.[2] Otherwise, some households may misuse the high feed-in tariff by storing energy from a utility company and sell the energy later. The problem defined in (17) is still difficult to solve because constraints (17e) and (17f) are neither linear nor convex.

To tackle this problem, we introduce new auxiliary binary variables $b_1(\tau,\boldsymbol{\omega}_k)$ and $b_2(\tau,\boldsymbol{\omega}_k)$ to indicate whether $q_1(\tau,\boldsymbol{\omega}_k)$ and $q_2(\tau,\boldsymbol{\omega}_k)$ are strictly positive or not, respectively. For example, we have $b_1(\tau,\boldsymbol{\omega}_k)=1$ if $q_1(\tau,\boldsymbol{\omega}_k)>0$, and $b_1(\tau,\boldsymbol{\omega}_k)=0$ otherwise. Next, we transform problem (17) as

$$\begin{aligned}\underset{\substack{\mathbf{e}(\tau,\boldsymbol{\omega}_k),\,q_0(\tau,\boldsymbol{\omega}_k),\\ q_1(\tau,\boldsymbol{\omega}_k),\,q_2(\tau,\boldsymbol{\omega}_k),\\ b_1(\tau,\boldsymbol{\omega}_k),\,b_2(\tau,\boldsymbol{\omega}_k),\\ \tau\in\mathcal{T}_t,\ k\in\mathcal{K}}}{\text{minimize}} \quad & \sum_{k\in\mathcal{K}}\mathbb{P}(\boldsymbol{\omega}_k)\sum_{\tau\in\mathcal{T}_t}\Big(p^e(\tau)(|H|-q_0(\tau,\boldsymbol{\omega}_k))\\ & -p^s(\tau)q_1(\tau,\boldsymbol{\omega}_k)\\ & -\big(p^s(\tau)-\eta\sum_{n\in\mathcal{B}^v(\tau)}\frac{\partial|V_n(\tau)|}{\partial E_b^x(\tau)}\big)q_2(\tau,\boldsymbol{\omega}_k)\Big)\end{aligned} \tag{18a}$$

$$\text{subject to}\quad b_1(\tau,\boldsymbol{\omega}_k)\geq\frac{q_1(\tau,\boldsymbol{\omega}_k)}{h},\quad \tau\in\mathcal{T}_t,\quad k\in\mathcal{K}, \tag{18b}$$

$$b_2(\tau,\boldsymbol{\omega}_k)\geq\frac{q_2(\tau,\boldsymbol{\omega}_k)}{G},\quad \tau\in\mathcal{T}_t,\quad k\in\mathcal{K}, \tag{18c}$$

$$b_1(\tau,\boldsymbol{\omega}_k)\leq\frac{q_0(\tau,\boldsymbol{\omega}_k)}{|H|},\quad \tau\in\mathcal{T}_t,\quad k\in\mathcal{K}, \tag{18d}$$

$$b_2(\tau,\boldsymbol{\omega}_k)\leq\frac{q_1(\tau,\boldsymbol{\omega}_k)}{h},\quad \tau\in\mathcal{T}_t,\quad k\in\mathcal{K}, \tag{18e}$$

$$b_1(\tau,\boldsymbol{\omega}_k),b_2(\tau,\boldsymbol{\omega}_k)\in\{0,1\},\quad \tau\in\mathcal{T}_t,\quad k\in\mathcal{K}, \tag{18f}$$

Constraints (9b) – (9e), (15), (17b) – (17d), and (17g),

where G is a positive constant and larger than the maximum of $q_2(\tau,\boldsymbol{\omega}_k)$. Constraints (18b), (18c), and (18f) yield $b_1(\tau,\boldsymbol{\omega}_k)=1$ and $b_2(\tau,\boldsymbol{\omega}_k)=1$ if $q_1(\tau,\boldsymbol{\omega}_k)$ and $q_2(\tau,\boldsymbol{\omega}_k)$ are strictly positive, respectively. Constraints (18b) and (18d) replace nonlinear constraint (17e) in problem (17). They guarantee that $q_1(\tau,\boldsymbol{\omega}_k)$ is strictly positive only if $q_0(\tau,\boldsymbol{\omega}_k)$ is at its maximum. Note that if $q_0(\tau,\boldsymbol{\omega}_k)<|H|$, we have $b_1(\tau,\boldsymbol{\omega}_k)=0$ according to constraints (18d) and (18f). Then, we can infer $q_1(\tau,\boldsymbol{\omega}_k)=0$ according to (18b). Similarly, constraints (18c) and (18e) replace nonlinear constraint (17f). They ensure that $q_2(\tau,\boldsymbol{\omega}_k)$ is strictly positive only if $q_1(\tau,\boldsymbol{\omega}_k)$ is at its maximum. Problem (18) is a mixed-integer program (MIP) and can be solved with an off-the-shelf optimization software such as MOSEK [44] or CPLEX [45]. We will discuss its computational complexity in Section IV.

We present the proposed energy consumption scheduling algorithm in Algorithm 1. The algorithm is executed at the beginning of each hour t by the ECS. The ECS first initializes the parameters and retrieves the pricing information and power flow analysis information from the utility company and the DNO, respectively (Lines 1-3). Then, the ECS constructs scenarios $\boldsymbol{\omega}_k, k\in\mathcal{K}$, according to historical data records of PV power generation (Line 4). Subsequently, problem (11) is solved when the objective function is a convex piecewise linear function, otherwise problem (18) is solved (Lines 5-9). The results are used to control the operation of the deferrable load and ESSs (Line 10). Finally, the ECS updates $E_i^r(t+1)$ and $s_l(t+1)$ to prepare for the scheduling for the next hour (Line 11).

[2]Under the current net metering programs of Ontario Hydro and Georgia Power, the discharged energy from an ESS can be used to support the load but cannot be compensated if used to export energy. Some utility companies (e.g., Georgia Power) require the households to install an additional meter for their PV units, such that the utility can determine whether the energy export comes from the PV units or not.

Algorithm 1 Energy consumption scheduling algorithm executed at the beginning of each time slot t by the ECS

1: Initialize $\mathcal{S}^d$, $\mathcal{S}^s$, $E_i^r(t), T_i^d, i\in\mathcal{S}^d$, $\mathcal{T}_t$, and $\mathcal{K}$.
2: Retrieve $p^e(\tau)$, $p^s(\tau)$, $\tau\in\mathcal{T}_t$ from the utility company through the communication network.
3: Retrieve η, h, $|V_n(\tau)|$, and $\sum_{n\in\mathcal{B}^v(\tau)}\frac{\partial|V_n(\tau)|}{\partial E_b^x(\tau)}$ from the DNO.
4: Construct scenarios $\omega_k, k\in\mathcal{K}$, according to the expected power generation from the PV units under different weather conditions (e.g., sunny, cloudy, rainy).
5: **if** $p^s(\tau)\leq p^e(\tau)$, $\tau\in\mathcal{T}_t$ **then**
6: Solve problem (11) to obtain the scheduling results.
7: **else**
8: Solve problem (18) to obtain the scheduling results.
9: **end if**
10: Control the operation of the deferrable load and ESSs according to the scheduling results.
11: Update $E_i^r(t+1), s_l(t+1)$ according to (5) and (6), respectively.

IV. Performance Evaluation

In this section, we present simulation results and assess the performance of the proposed energy consumption scheduling algorithm. We compare our proposed algorithm with the algorithm in [19], which we refer to as the HDA (HVAC load Direct Activation) algorithm. Both the HDA algorithm and our proposed algorithm consider residential load management in the presence of the voltage rise problem. While our proposed algorithm schedules household loads based on a cost function, the HDA algorithm is based on a real-time voltage signal. The HDA algorithm activates the idle HVAC load (e.g., water heater) when a voltage rise is detected. We also compare our proposed algorithm with a benchmark algorithm, where the ECS is not deployed and the deferrable load is not controlled.

We consider the 33 bus radial distribution test system [25]. We assume there are 10-40 households on each bus and each household has installed PV units and ESSs. The households have deferrable loads as shown in Table I. The daily consumption of the must-run load for each household is randomly selected from the interval $[6,18]$ kWh and the hourly consumption profile is generated according to [46]. The hourly profile of PV power generation is obtained from [47]. The daily energy generation from PV units for each household is randomly selected from the interval $[8,24]$ kWh. We denote

TABLE I
LIST OF DEFERRABLE LOADS

Load	Energy Usage (kWh)	Task Deadline
Dish washer	$[0, 4]$	[6 pm, 8 pm]
Water heater	$[0, 10]$	[7 pm, 12 am]
Clothes dryer	$[0, 3]$	[10 pm, 12 am]

the percentage of deferrable load by β. We have

$$\beta = \frac{\sum_{\tau\in\mathcal{T}}\sum_{i\in\mathcal{S}^d} E_i^d(\tau)}{\sum_{\tau\in\mathcal{T}}\left(\sum_{i\in\mathcal{S}^d} E_i^d(\tau) + \sum_{j\in\mathcal{S}^m} E_j^m(\tau)\right)} \times 100\%.$$

We consider the case where the household is equipped with a small-scale local battery system. The capacity of the battery is 4 kWh [22]. The maximum charged and discharged energy in one hour is 1 kWh and -1 kWh, respectively.

We use two pricing schemes in order to analyze the two cases presented in Sections III-C and III-D. We denote the first pricing scheme by Price1, where we have $p^s(\tau) = p^e(\tau)$. Price1 is similar to the TOU net metering program of Southern California Edison [48]. The second pricing scheme is denoted by Price2, where the energy selling price is obtained from [8]. Price2 represents the case when the utility company sets the feed-in tariff higher than the price of energy consumption, as Ontario Hydro does.

Our simulations cover a period of 30 days. The number of sunny, cloudy, and rainy days is 23, 4, and 3, respectively. Note that different PV units may experience different weather conditions, especially when the distribution network covers a large geographical area. Moreover, because of the elevation angle of the sun, even on sunny days, some PV units may not be able to produce energy at their full capacity. Hence, for the sunny days, we assume 85% of the PV units generate energy with their full capacity and the remaining 15% of the PV units produce power at 60% of the capacity in each time slot.

We first perform the power flow analysis with the Newton-Raphson method and obtain the partial derivatives of the voltage magnitudes with respect to household energy export [14], [26], [27]. We assume $\eta = 2\times10^{-4}$ in (3) for simulation purpose. The value of η is selected such that the external cost is comparable to the monetary cost. We consider an arbitrary household on bus $b=18$ in the 33 bus radial distribution test system (cf. Fig. 2). The line impedances and distances between buses are obtained from [25].

A. Computational Complexity

We investigate the computational complexity of the proposed algorithm in Table II. We use the optimization software MOSEK to solve LP problem (11) and MIP problem (18). The run time is evaluated with a desktop computer which has a quad-core processor and 16 gigabyte memory. For an MIP problem, MOSEK uses the branch-and-cut method and is able to find an ϵ-optimal solution within a reasonable time. Here, ϵ denotes the optimality gap (i.e., the gap between the obtained objective value and the optimal objective value does not exceed a small value ϵ). The run time was measured for $\epsilon = 0.01$.

As shown in Table II, an ϵ-optimal solution can be obtained with MOSEK within a short period of time.

TABLE II
COMPUTATIONAL COMPLEXITY TABLE FOR THE PROPOSED ALGORITHM

Pricing scheme	Price1	Price2
Cost function	convex	non-convex
Formulation	problem (11)	problem (18)
Formulation type	LP	MIP
Continuous variables	3456	4032
Binary variables	0	576
Constraints	3870	4718
Run time (seconds)	0.189	7.654

We note that, in practice, a smart meter typically has much less computational resources compared to a desktop computer. For example, the Atmel smart meter [49] uses an ARM Cortex CPU with a bus frequency of 120 MHz and the size of the memory is 2 MB. Hence, for current smart meters, it is difficult to implement the load scheduling algorithms which require to solve complicated optimization problems. On the other hand, we expect that future smart meters will have more computational resources, considering that the prices of CPU and memory are constantly dropping. Moreover, new computational infrastructure (e.g., cloud computing) can be leveraged to tackle this problem. For an ECS, its task can be divided into three steps. First, the ECS needs to retrieve the values of required energy and task deadline from each appliance. These values are used as inputs of the optimization problem for load scheduling. Second, the optimization problem is solved to determine the operating schedule of different appliances. Third, the ECS uses the results to control the appliances. A smart meter seems to be an ideal candidate to perform the first and the third steps. However, it may not be necessary for the smart meter to perform the second step. Instead, the smart meter can offload the computational tasks to one or multiple servers in a cloud platform (e.g., Microsoft Azure [50]), which has abundant computational resources. After the servers have solved the optimization problem, the results can be sent to the ECS via a communication infrastructure.

B. Performance Gains for Voltage Rise Mitigation

We evaluate the performance of our proposed algorithm and the HDA algorithm [19] for tackling the voltage rise problem. We use the Newton-Raphson method to calculate the bus voltage magnitude for each time slot after load shifting. Fig. 5 shows the voltage magnitude profile of bus 18 in Fig. 2. Bus 18 is selected as it has a longer distance from the substation compared to other buses and experiences a larger voltage variation (voltage drop and voltage rise) when the power flow changes. As shown in Fig. 5, our proposed algorithm avoids the voltage rise problem for households during the noon period (10:00 - 14:00). The proposed algorithm outperforms the HDA algorithm for two reasons. First, we jointly considered the residential load and ESSs in our model. Second, for the HDA algorithm, the tasks of some deferrable loads (e.g., dish washers, clothes dryers) may have already been finished, when voltage rise happens. These loads may not be activated in this case. Note we consider Price2 in Fig. 5 but the proposed

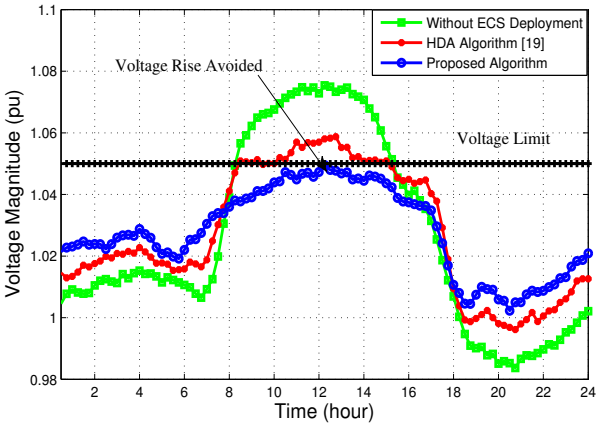

Fig. 5. Comparison of the household voltage magnitude profile of the proposed algorithm and the HDA algorithm [19]. The voltage magnitude is shown in per unit (pu). The base value of pu is the standard voltage (e.g., 120 volt for households). The voltage limit is 1.05 pu. In the proposed algorithm, the voltage rise is avoided by reducing the household energy export during hours with high solar power generation.

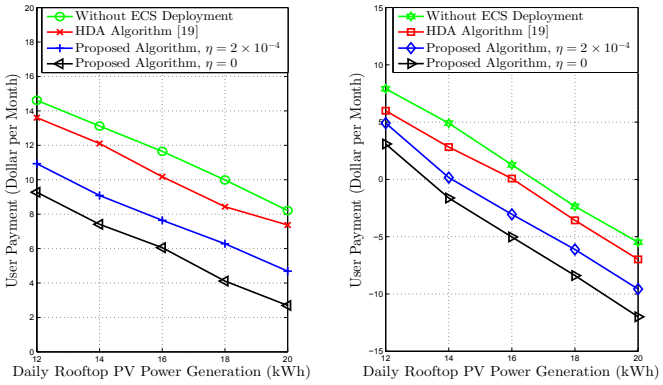

(a) User Payment under Price1 (b) User Payment under Price2

Fig. 6. Comparison of the monthly electricity bill for different amount of daily rooftop PV power generation.

algorithm achieves a similar performance in terms of voltage rise mitigation for Price1.

C. Benefits Regarding Electricity Bill and PAR

Fig. 6 shows the monthly electricity bill for different amount of daily rooftop PV power generation. When $\eta = 2 \times 10^{-4}$, the proposed algorithm reduces the user payment from \$11.6 to \$7.5 when the daily generation is 16 kWh under Price1. The user payment decreases from \$1.3 to $-$\$3.2 under Price2. For the proposed algorithm, we consider two cases, namely $\eta = 2 \times 10^{-4}$ and $\eta = 0$. Note that the value of η can be tuned in the proposed algorithm to adjust the weight on reducing the voltage rise magnitude and reducing the electricity bill. When $\eta = 0$, the ECS neglects the potential voltage rise problem and only aims to reduce the electricity bill. As shown in Fig. 6, the bill is reduced when $\eta = 0$, compared to the case when $\eta = 2 \times 10^{-4}$. In particular, the bill is decreased from \$7.5 to \$6.1 when η is decreased from 2×10^{-4} to 0 under Price1. Under Price2, the bill is decreased from $-$\$3.2 to $-$\$4.9. The saving of load shifting depends on the pricing scheme used by the utility company. For example, the Southern California Edison has recently introduced a residential TOU pricing scheme where the price during peak hours is 4.18 times higher than the price during the night hours [51]. The load shifting can achieve a higher saving on electricity bill in this case. Moreover, if ECSs are widely installed, the total saving can be significant, considering the large numbers of households. In Fig. 6, the electricity bill is the highest when the ECS is not deployed because the loads are not shifted during the expensive peak hours. The HDA algorithm reduces the bill as some of the HVAC appliances finish their tasks during high solar radiation hours and consume less during peak hours. Our proposed algorithm further reduces the bill as more loads are shifted from peak hours.

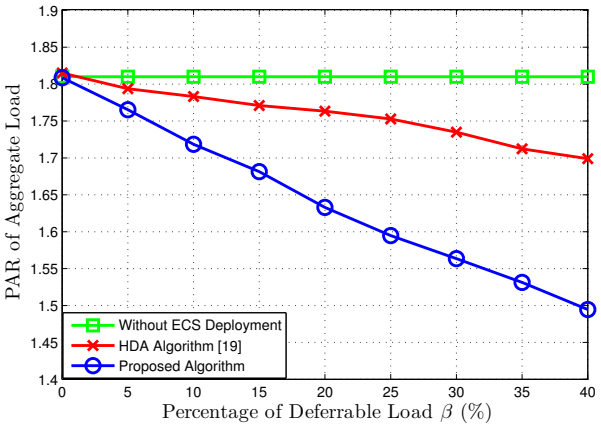

Fig. 7. Comparison of the aggregate load peak-to-average ratio (PAR) of the proposed algorithm and the HDA algorithm from [19].

Fig. 7 shows the PAR of the aggregate load versus the percentage of deferrable load β. The proposed algorithm reduces the PAR from 1.81 to 1.49 when $\beta = 40\%$. As β increases from 0% to 40%, the PAR decreases because more deferrable loads can be shifted from peak hours to off-peak hours.

D. The Impact of Forecast Error

Forecast error refers to the difference between the forecasted value and the actual value of the PV energy generation or the load. Forecast errors persist as both solar radiation and load are intrinsically stochastic. As forecasted values are used in the proposed algorithm, the forecast errors may degrade its performance. We use the mean absolute percentage error (MAPE) to measure the forecast error, which is defined as $\frac{1}{2T}\sum_{t\in\mathcal{T}}\left(\frac{|\hat{E}^g(t)-E^g(t)|}{E^g(t)} + \frac{|\sum_{j\in\mathcal{S}^m}\hat{E}^m_j(t)-\sum_{j\in\mathcal{S}^m}E^m_j(t)|}{\sum_{j\in\mathcal{S}^m}E^m_j(t)}\right)$, where $\hat{E}^g(t)$ and $\sum_{j\in\mathcal{S}^m}\hat{E}^m_j(t)$ are the forecasted values of the energy generation of the PV unit and the energy consumption of must-run loads in time slot $t \in \mathcal{T}$, respectively. We adopt different scenarios to model the uncertainty in energy generation. Therefore, the forecasted energy generation is calculated as $\hat{E}^g(t) = \sum_{k\in\mathcal{K}}\mathbb{P}(\boldsymbol{\omega}_k)\hat{E}^g(t,\boldsymbol{\omega}_k)$, where $\hat{E}^g(t,\boldsymbol{\omega}_k)$ is the forecasted energy generation under scenario $\boldsymbol{\omega}_k$ in time slot t. In Figs. 8 and 9, we allocate the same

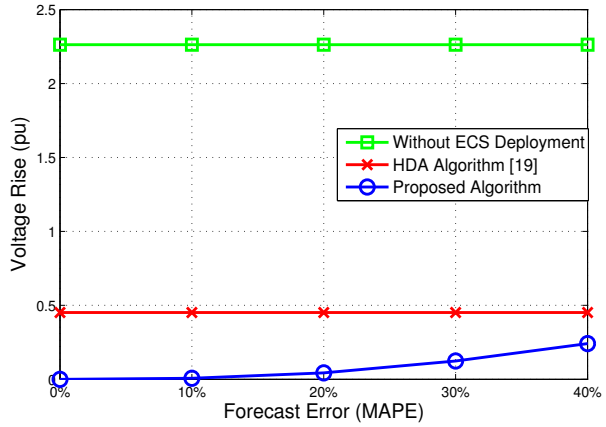

Fig. 8. The voltage rise versus the forecast error. The y-axis is the summation of the voltage rise over time slots and buses, which can be written as $\sum_{t\in\mathcal{T}}\sum_{n\in\mathcal{B}}(V_n(t)-\bar{V})^+$, where $\bar{V}$ is the upper limit of the allowed voltage variation and $(\cdot)^+=\max\{\cdot,0\}$.

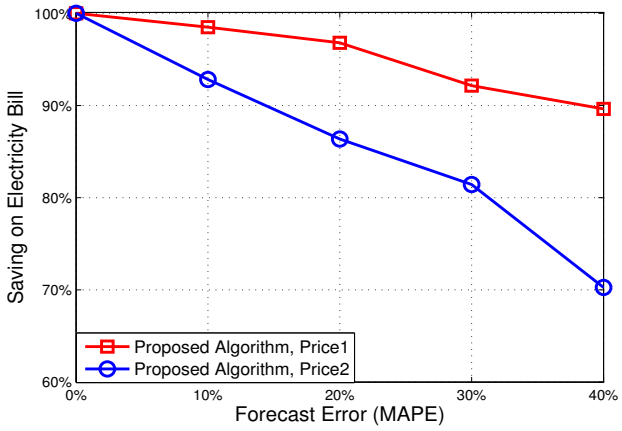

Fig. 9. The saving on the monthly electricity bill versus the forecast error. The y-axis is the percentage of the saving. The baseline of the percentage is the saving when the energy generation and loads are perfectly known. The saving decreases as the forecast error increases.

MAPE for the energy generation and must-run load. This is because the gap between the energy generation and must-run load affects the load shifting. We are particularly interested in the performance of the proposed algorithm under different forecast errors for this gap. Furthermore, we consider the summation of the voltage rise magnitude at different buses for different time slots, i.e., $\sum_{t\in\mathcal{T}}\sum_{n\in\mathcal{B}}(V_n(t)-\bar{V})^+$, as a metric to evaluate the severity of the voltage rise problem. We have $\bar{V}=1.05$ pu as we consider the ANSI C84.1 standard [15] which is used in North America. Fig. 8 shows the voltage rise versus the forecast error. As illustrated in Fig. 8, the performance of the proposed algorithm in mitigating the voltage rise problem degrades when the forecast error is significant. However, our proposed algorithm is able to reduce the magnitude of voltage rise even in the presence of forecast error, since the ECS tends to shift the load to high solar radiation hours. Note that the voltage magnitude is affected by the load profile of multiple households while each household may overestimate or underestimate its energy

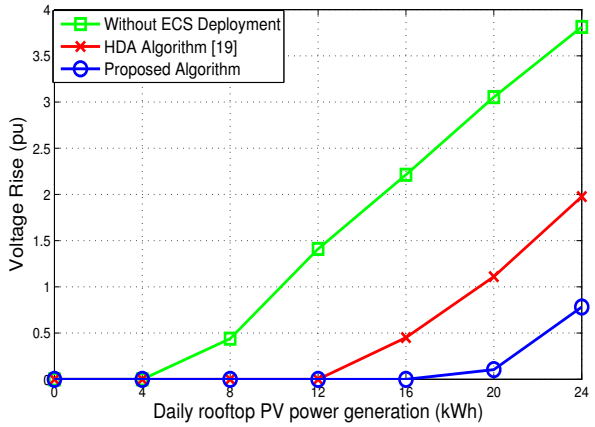

Fig. 10. The voltage rise versus the daily power generation of the rooftop PV unit. The y-axis is the summation of the voltage rise over time slots and buses, which can be written as $\sum_{t\in\mathcal{T}}\sum_{n\in\mathcal{B}}(V_n(t)-\bar{V})^+$. We choose $\eta=2\times10^{-4}$.

generation and consumption. The forecast errors of different households sometimes have opposite impacts on the voltage magnitude.

The forecast error may also degrade the ability of the proposed algorithm to reduce the monthly electricity bill of the users. We use the saving on the electricity bill as a metric of performance. The saving is defined as the difference between the monthly bill of the user for the proposed algorithm and the bill in the case when the ECS is not deployed. To have a baseline to compare with, we consider the case in which the energy generation and loads are perfectly known. For the case with complete information of generation and demand, we can achieve the maximum energy saving. In the following, we calculate the saving under different forecast errors. The saving as a function of the forecast error is shown in Fig. 9. Results show that the saving decreases as the forecast error increases. However, the saving is still considerable in the presence of forecast error. This is because the ECS tends to shift the load from peak hours when the energy consumption price is high to off-peak hours.

E. The Impact of PV Power Generation and Parameter η

The power generation of the PV units is important to the voltage rise problem. In this section, we study the performance of the proposed algorithm for different daily power generations of the rooftop PV units and different values of parameter η. Fig. 10 depicts the voltage rise magnitude versus the daily power generation of rooftop PV units under the proposed algorithm. As shown in the figure, the voltage rise magnitude increases as the power generation of rooftop PV units increases. Fig. 11 shows the magnitude of the voltage rise versus parameter η. When parameter η is small, the ECS does not shift load to mitigate the voltage rise. As parameter η increases, the voltage rise decreases since the ECS tends to put more weight on the voltage rise mitigation rather than reducing the electricity bill. The daily energy generation of PV units is assumed to be 16 kWh in Fig. 11.

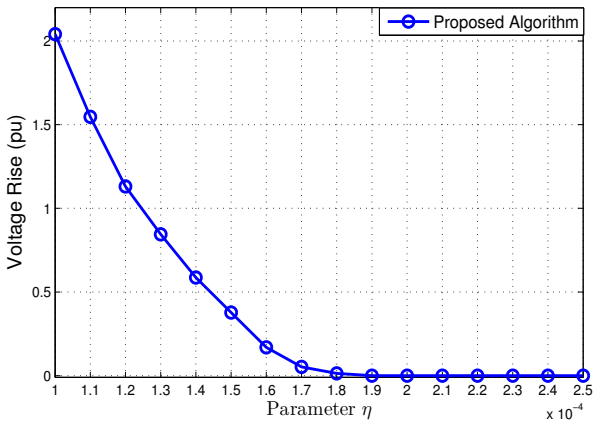

Fig. 11. The impact of parameter η. The y-axis is the summation of the voltage rise $\sum_{t\in\mathcal{T}}\sum_{n\in\mathcal{B}}(V_n(t)-\bar{V})^+$. Note that η is a parameter of the proposed algorithm. The performance of the cases when the ECS is not installed or the HDA algorithm is used are not affected by η.

V. Conclusion

In this paper, we proposed a residential energy consumption scheduling algorithm for areas with high penetration of rooftop PV units. The proposed algorithm aimed to jointly shave the peak load and mitigate the voltage rise problem during high solar radiation hours. We modeled the adverse effect of excessive energy export on causing abnormally high voltage magnitude as an external cost based on the power flow analysis. A stochastic program was formulated to minimize the household electricity bill and the external cost under the uncertainty in PV power generation. The objective function was convex piecewise linear when the feed-in tariff did not exceed the energy consumption price. Otherwise, the objective function was non-convex piecewise linear and we transformed the problem into an MIP. Simulation results confirmed that the proposed algorithm reduced the electricity bill and the PAR of the aggregate load. The algorithm is also effective for mitigating the voltage rise problem caused by high penetration of rooftop PV units. An interesting topic for the future work is the joint consideration of residential load scheduling and real-time control of the ESSs and PV inverters to make the algorithm more resilient to inaccurate forecast of energy generation and load.

References

[1] G. Strbac, "Demand side management: Benefits and challenges," *Energy Policy*, vol. 36, no. 12, pp. 4419–4426, Dec. 2008.

[2] A. H. Mohsenian-Rad, V.W.S. Wong, J. Jatskevich, R. Schober, and A. Leon-Garcia, "Autonomous demand side management based on game-theoretic energy consumption scheduling for the future smart grid," *IEEE Trans. on Smart Grid*, vol. 1, no. 3, pp. 320–331, Dec. 2010.

[3] A. Conejo, J. Morales, and L. Baringo, "Real-time demand response model," *IEEE Trans. on Smart Grid*, vol. 1, no. 3, pp. 236–242, Dec. 2010.

[4] N. Li, L. Chen, and S. H. Low, "Optimal demand response based on utility maximization in power networks," in *Proc. of IEEE PES General Meeting*, Detroit, MI, July 2011.

[5] P. Samadi, H. Mohsenian-Rad, R. Schober, and V.W.S. Wong, "Tackling the load uncertainty challenges for energy consumption scheduling in smart grid," *IEEE Trans. on Smart Grid*, vol. 4, no. 2, pp. 1007–1016, June 2013.

[6] P. Samadi, H. Mohsenian-Rad, V.W.S. Wong, and R. Schober, "Real-time pricing for demand response based on stochastic approximation," *IEEE Trans. on Smart Grid*, vol. 5, no. 2, pp. 789–798, Mar. 2014.

[7] Net Metering in the Illinois State of United States, Available at: www.illinoisattorneygeneral.gov/environment/netmetering.html.

[8] Feed-in tariff in Province of Ontario in Canada, Available at: http://fit.powerauthority.on.ca/what-feed-tariff-program.

[9] A. Pedrasa, T. D. Spooner, and I. F. MacGill, "Coordinated scheduling of residential distributed energy resources to optimize smart home energy services," *IEEE Trans. on Smart Grid*, vol. 1, no. 2, pp. 134–143, Nov. 2010.

[10] I. Atzeni, L. G. Ordonez, G. Scutari, D. P. Palomar, and J. R. Fonollosa, "Demand-side management via distributed energy generation and storage optimization," *IEEE Trans. on Smart Grid*, vol. 4, no. 2, pp. 866–876, June 2013.

[11] C. O. Adika and L. Wang, "Autonomous appliance scheduling for household energy management," *IEEE Trans. on Smart Grid*, vol. 5, no. 2, pp. 673–682, Mar. 2014.

[12] R. A. Walling, R. Saint, R. C. Dugan, J. Burke, and L. A. Kojovic, "Summary of distributed resources impact on power delivery systems," *IEEE Trans. on Power Delivery*, vol. 23, no. 3, pp. 1636–1644, July 2008.

[13] R. Tonkoski, D. Turcotte, and T. El-Fouly, "Impact of high PV penetration on voltage profiles in residential neighborhoods," *IEEE Trans. on Sustainable Energy*, vol. 3, no. 3, pp. 518–527, May 2012.

[14] J. D. Glover, M. S. Sarma, and T. Overbye, *Power System Analysis and Design, 5th Edition*. Cengage Learning, 2011.

[15] American National Standard for Electric Power Systems and Equipment Voltage Ratings, American National Standards Institute (ANSI) C84.1, 2006.

[16] J. von Appen, M. Braun, T. Stetz, K. Diwold, and D. Geibel, "Time in the sun: The challenge of high PV penetration in the German electric grid," *IEEE Power and Energy Magazine*, vol. 11, no. 2, pp. 55–64, Mar. 2013.

[17] T. Stetz, F. Marten, and M. Braun, "Improved low voltage grid-integration of photovoltaic systems in Germany," *IEEE Trans. on Sustainable Energy*, vol. 4, no. 2, pp. 534–542, Apr. 2013.

[18] "German Renewable Energy Sources Act (Erneuerbare-Energien-Gesetz)," Available at: http://www.erneuerbare-energien.de/EE/Navigation/DE/Gesetze/Das_EEG/das_eeg.html.

[19] S. J. Steffel, P. R. Caroselli, A. M. Dinkel, J. Q. Liu, R. N. Sackey, and N. R. Vadhar, "Integrating solar generation on the electric distribution grid," *IEEE Trans. on Smart Grid*, vol. 3, no. 2, pp. 878–886, June 2012.

[20] X. Liu, A. Aichhorn, L. Liu, and H. Li, "Coordinated control of distributed energy storage system with tap changer transformers for voltage rise mitigation under high photovoltaic penetration," *IEEE Trans. on Smart Grid*, vol. 3, no. 2, pp. 897–906, June 2012.

[21] M. J. E. Alam, K. M. Muttaqi, and D. Sutanto, "Distributed energy storage for mitigation of voltage-rise impact caused by rooftop solar PV," in *Proc. of IEEE PES General Meeting*, San Diego, CA, July 2012.

[22] J. von Appen, T. Stetz, M. Braun, and A. Schmiegel, "Local voltage control strategies for PV storage systems in distribution grids," *IEEE Trans. on Smart Grid*, vol. 5, no. 2, pp. 1002–1009, Mar. 2014.

[23] E. Yao, P. Samadi, V.W.S. Wong, and R. Schober, "Tackling the photovoltaic integration challenge in the distribution network with deferrable load," in *Proc. of IEEE SmartGridComm*, Vancouver, Canada, Oct. 2013.

[24] IEEE 1547 Standard for Interconnecting Distributed Resources with Electric Power Systems, http://grouper.ieee.org/groups/scc21/1547/1547_index.html.

[25] R. S. Rao, K. Ravindra, K. Satish, and S. V. L. Narasimham, "Power loss minimization in distribution system using network reconfiguration in the presence of distributed generation," *IEEE Trans. on Power Systems*, vol. 28, no. 1, pp. 317–325, Feb. 2013.

[26] M. Brenna, E. D. Berardinis, F. Foiadelli, G. Sapienza, and D. Zaninelli, "Voltage control in smart grids: An approach based on sensitivity theory," *Journal of Electromagnetic Analysis and Applications*, vol. 2, no. 1, pp. 669–678, Dec. 2006.

[27] K. M. Rogers, R. Klump, H. Khurana, A. A. Aquino-Lugo, and T. J. Overbye, "An authenticated control framework for distributed voltage support on the smart grid," *IEEE Trans. on Smart Grid*, vol. 1, no. 1, pp. 40–47, June 2010.

[28] Power system simulator PowerWorld, Available at: www.powerworld.com.

[29] N. G. Mankiw, *Principle of Economics, 6th edition*. Cengage Learning, 2011.

[30] R. Tonkoski, L. A. C. Lopes, and T. H. M. El-Fouly, "Coordinated active power curtailment of grid connected PV inverters for overvoltage prevention," *IEEE Trans. on Smart Grid*, vol. 2, no. 2, pp. 139–147, Apr. 2011.
[31] L. Yu, D. Czarkowski, and F. de León, "Optimal distributed voltage regulation for secondary networks with DGs," *IEEE Trans. on Smart Grid*, vol. 3, no. 2, pp. 959–967, June 2012.
[32] S. Bolognani and S. Zampieri, "A distributed control strategy for reactive power compensation in smart microgrids," *IEEE Trans. on Automatic Control*, vol. 58, no. 11, pp. 2818–2833, Nov. 2013.
[33] R. H. Coase, "The problem of social cost," *Journal of Law and Economics*, vol. 3, no. 1, pp. 1–44, Oct. 1960.
[34] A. D. Owen, "Renewable energy: Externality costs as market barriers," *Energy Policy*, vol. 34, no. 5, pp. 632–642, Mar. 2006.
[35] P. Rafaj and S. Kypreos, "Internalisation of external cost in the power generation sector: Analysis with global multi-regional MARKAL model," *Energy Policy*, vol. 35, no. 2, pp. 828–843, Feb. 2007.
[36] X. Li and C. W. Yu, "Impacts of emission trading on carbon, electricity and renewable markets: A review," in *Proc. of IEEE PES General Meeting*, Minneapolis, MN, Jul. 2010.
[37] Q. Chen, C. Kang, Q. Xia, and D. Kirschen, "Optimal flexible operation of a CO_2 capture power plant in a combined energy and carbon emission market," *IEEE Trans. on Power Systems*, vol. 27, no. 3, pp. 1602–1609, Aug. 2012.
[38] S. Boyd and L. Vandenberghe, *Convex Optimization*. Cambridge University Press, 2004.
[39] A. Shapiro, D. Dentcheva, and A. Ruszczynski, *Lectures on Stochastic Programming: Modeling and Theory*. SIAM, 2009.
[40] A. Yona, T. Senjyu, A. Y. Saber, T. Funabashi, H. Sekine, and C. H. Kim, "Application of neural network to 24-hour-ahead generating power forecasting for pv system," in *Proc. of IEEE PES General Meeting*, Pittsburgh, PA, Jul. 2008.
[41] E. Lorenz, J. Hurka, D. Heinemann, and H. G. Beyer, "Irradiance forecasting for the power prediction of grid-connected photovoltaic systems," *IEEE Journal of Selected Topics in Applied Earth Observations and Remote Sensing*, vol. 2, no. 1, pp. 2–10, Mar. 2009.
[42] P. Bachera, H. Madsena, and H. A. Nielsen, "Online short-term solar power forecasting," *Solar Energy*, vol. 83, no. 10, pp. 1772–1783, Oct. 2009.
[43] Solar purchase program in Georgia state in the United States, Available at: http://www.georgiapower.com/pricing/residential/residential-tariffs.cshtml.
[44] Optimization software MOSEK, Available at: http://www.mosek.com/.
[45] Optimization software CPLEX, Available at: http://www-01.ibm.com/software/commerce/optimization/cplex-optimizer/.
[46] J. A. Jardini, C. M. V. Tahan, M. R. Gouvea, S. U. Ahn, and F. M. Figueiredo, "Daily load profiles for residential, commercial and industrial low voltage consumers," *IEEE Trans. on Power Delivery*, vol. 15, no. 1, pp. 375–380, Jan. 2000.
[47] Solar Data from National Renewable Energy Laboratory (NREL), Available at: http://www.nrel.gov/rredc/solar_data.html.
[48] Southern California Edison Net Metering Program, Available at: https://www.sce.com/NR/sc3/tm2/pdf/ce158-12.pdf.
[49] Atmel Smart Metering Solutions, Available at: http://www.atmel.com/applications/Smart_Energy/default.aspx.
[50] Microsoft Azure: Cloud Computing Platform, Available at: http://azure.microsoft.com.
[51] Southern California Edison Residential Time of Use Rate Plan, Available at: https://www.sce.com/wps/portal/home/residential/rates/residential-plan/tou.

Enxin Yao (S'11) received the B.S. and the M.S. degrees both from Peking University, Beijing, China in 2008 and 2011, respectively. He is currently a Ph.D. candidate in the Department of Electrical and Computer Engineering, the University of British Columbia, Vancouver, Canada. His research is in the area smart grid, with a focus on demand side management and electric vehicle frequency regulation service.

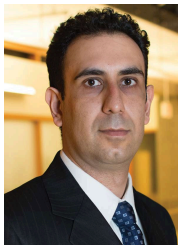

Pedram Samadi (S'09) received the B.Sc. and the M.Sc. degrees both from Isfahan University of Technology, Isfahan, Iran in 2006 and 2009, respectively. He also received the Ph.D. degree from the Department of Electrical and Computer Engineering, the University of British Columbia, Vancouver, Canada in 2015. His research interests are in the area of smart grid and especially demand side management.

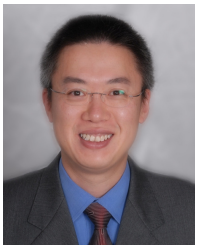

Vincent W.S. Wong (SM'07) received the B.Sc. degree from the University of Manitoba, Winnipeg, MB, Canada, in 1994, the M.A.Sc. degree from the University of Waterloo, Waterloo, ON, Canada, in 1996, and the Ph.D. degree from the University of British Columbia (UBC), Vancouver, BC, Canada, in 2000. From 2000 to 2001, he worked as a systems engineer at PMC-Sierra Inc. He joined the Department of Electrical and Computer Engineering at UBC in 2002 and is currently a Professor. His research areas include protocol design, optimization, and resource management of communication networks, with applications to wireless networks, smart grid, and the Internet. Dr. Wong is an Editor of the *IEEE Transactions on Communications*. He has served on the editorial boards of *IEEE Transactions on Vehicular Technology* and *Journal of Communications and Networks*. He has served as a Technical Program Co-chair of *IEEE SmartGridComm'14*, as well as a Symposium Co-chair of *IEEE SmartGridComm'13* and *IEEE Globecom'13*. He received the 2014 UBC Killam Faculty Research Fellowship. He is the Chair of the IEEE Communications Society Emerging Technical Sub-Committee on Smart Grid Communications and IEEE Vancouver Joint Communications Chapter.

Robert Schober (S'98, M'01, SM'08, F'10) was born in Neuendettelsau, Germany, in 1971. He received the Diplom (Univ.) and the Ph.D. degrees in electrical engineering from the University of Erlangen-Nuermberg in 1997 and 2000, respectively. From May 2001 to April 2002 he was a Postdoctoral Fellow at the University of Toronto, Canada, sponsored by the German Academic Exchange Service (DAAD). Since May 2002 he has been with the University of British Columbia (UBC), Vancouver, Canada, where he is now a Full Professor. Since January 2012 he is an Alexander von Humboldt Professor and the Chair for Digital Communication at the Friedrich Alexander University (FAU), Erlangen, Germany. His research interests fall into the broad areas of Communication Theory, Wireless Communications, and Statistical Signal Processing.

Dr. Schober received several awards for his work including the 2002 Heinz Maier–Leibnitz Award of the German Science Foundation (DFG), the 2004 Innovations Award of the Vodafone Foundation for Research in Mobile Communications, the 2006 UBC Killam Research Prize, the 2007 Wilhelm Friedrich Bessel Research Award of the Alexander von Humboldt Foundation, the 2008 Charles McDowell Award for Excellence in Research from UBC, a 2011 Alexander von Humboldt Professorship, and a 2012 NSERC E.W.R. Steacie Fellowship. In addition, he received best paper awards from the German Information Technology Society (ITG), the European Association for Signal, Speech and Image Processing (EURASIP), *IEEE WCNC 2012*, *IEEE Globecom 2011*, *IEEE ICUWB 2006*, the *International Zurich Seminar on Broadband Communications*, and *European Wireless 2000*. Dr. Schober is a Fellow of the Canadian Academy of Engineering and a Fellow of the Engineering Institute of Canada. He is currently the Editor-in-Chief of the *IEEE Transactions on Communications*.